

Electron Temperature Profile Dependence on the Recycling Rate in the Lithium Tokamak Experiment

Craig Michael Jacobson

Advisors: R. Majeski and B. LeBlanc

Committee: P. Efthimion, R. Kaita, and D. Stotler

September 25, 2009

Introduction

The search for suitable materials for the first wall is an important area of research in fusion science. As power loads for a reactor are predicted to be on the order of 100 MW m^{-2} , the first wall should have a high thermal conductivity and an ability to withstand large heat fluxes. The first wall should also not be a source of detrimental impurities. Traditionally, solid materials such as carbon, tungsten, beryllium, and molybdenum have been used for the first wall. While high-Z materials have higher sputtering thresholds, high-Z impurities can cause large radiative losses to the plasma. Wall damage is another issue, since solid walls slowly erode as they interact with plasma. As most fusion research focuses on using deuterium-tritium reactions for power production, the first wall should be able to withstand high-energy neutron flux [1]. The combination of plasma and neutron fluences strongly limits the lifetime of any solid used as a plasma-facing component.

Liquid metals are a viable alternative to high-Z solids. Recently, attention has been focused on liquid lithium as a first wall option. A liquid wall has the advantage of being self-healing. Since it has a low ionization potential, lithium from the first wall does not deeply penetrate into the plasma, but is instead rapidly redeposited on the wall. Lithium which does enter the core plasma has $Z = 3$, and does not cause large levels of radiation. Lithium can also be used to breed tritium for use in a D-T reactor.

Perhaps one of the best features of the use of liquid lithium for a first wall is that it leads to large reductions in recycling. This is the process by which plasma ions that diffuse out of the plasma become neutralized by interaction with the first wall, and then re-enter the plasma as neutrals. The reduction in recycling is due to the ability of lithium to form hydrides when exposed to hydrogen isotope plasmas up to the point when lithium fully reacts with the hydrogen isotopes present [2]. While recycling helps maintain the plasma's particle inventory, these neutrals usually have very low energies; thus their reintroduction to the plasma edge has a cooling effect. The edge temperature is brought down, increasing the thermal gradient, which can drive instabilities and degrade confinement. Lithium first walls allow a means of improving confinement, core temperature, and other measures of plasma performance. As shown in Figure 1, computational models indicate that lowering the recycling rate will flatten the electron temperature profile. Significant effects are expected for recycling coefficients of approximately 50%. The presence of lithium walls is predicted to result in more stable plasmas with better energy confinement, which are crucial for developing a viable fusion reactor [3].

Previous experiments have studied the effects of using lithium plasma facing components. TFTR conditioned a graphite limiter with lithium pellet deposition to increase τ_E , Q , and the Lawson triple product [4, 5]. Similar experiments in DIII-D also demonstrated increases in plasma performance [6]. While utilizing a liquid lithium toroidal tray limiter, CDX-U saw a reduction in the recycling rate, a strong reduction in impurities, an increase in the plasma core temperature, and a sixfold increase in the energy confinement time [7, 8, 9, 10, 11]. Figure 2 shows enhanced confinement over the ITER98P(y,1) scaling in CDX-U. Experiments

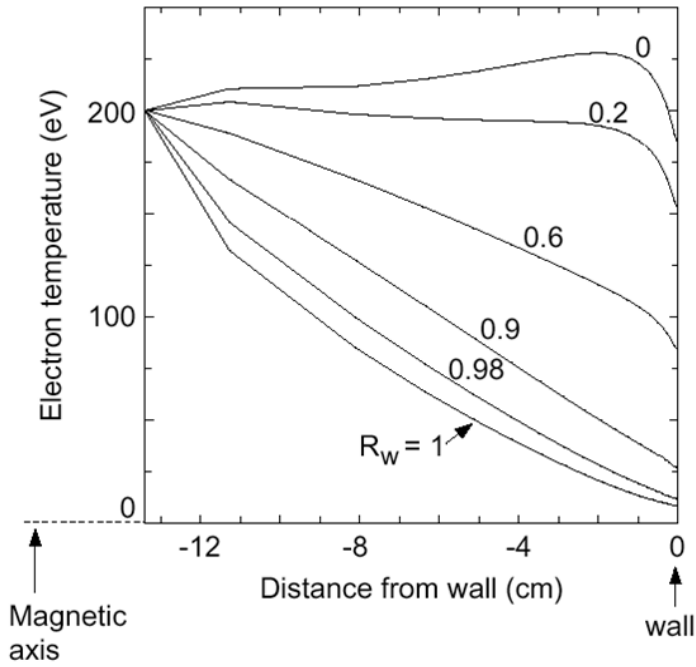


Figure 1: Calculated dependence of the electron temperature profile on the recycling coefficient at the wall R_w for a CDX-U equilibrium using UEDGE. T_e and T_i are fixed at 200 eV at the plasma center.

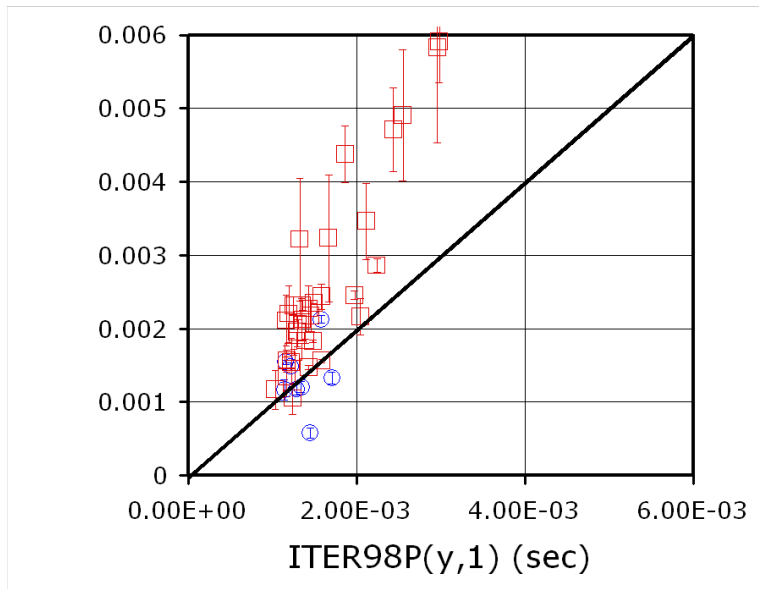


Figure 2: Experimentally measured confinement times for discharges with lithium coated walls on CDX-U compared to the ITER98P(y,1) scaling. Discharges without active lithium heating and evaporation appear as blue circles; discharges with active evaporation are shown as red squares.

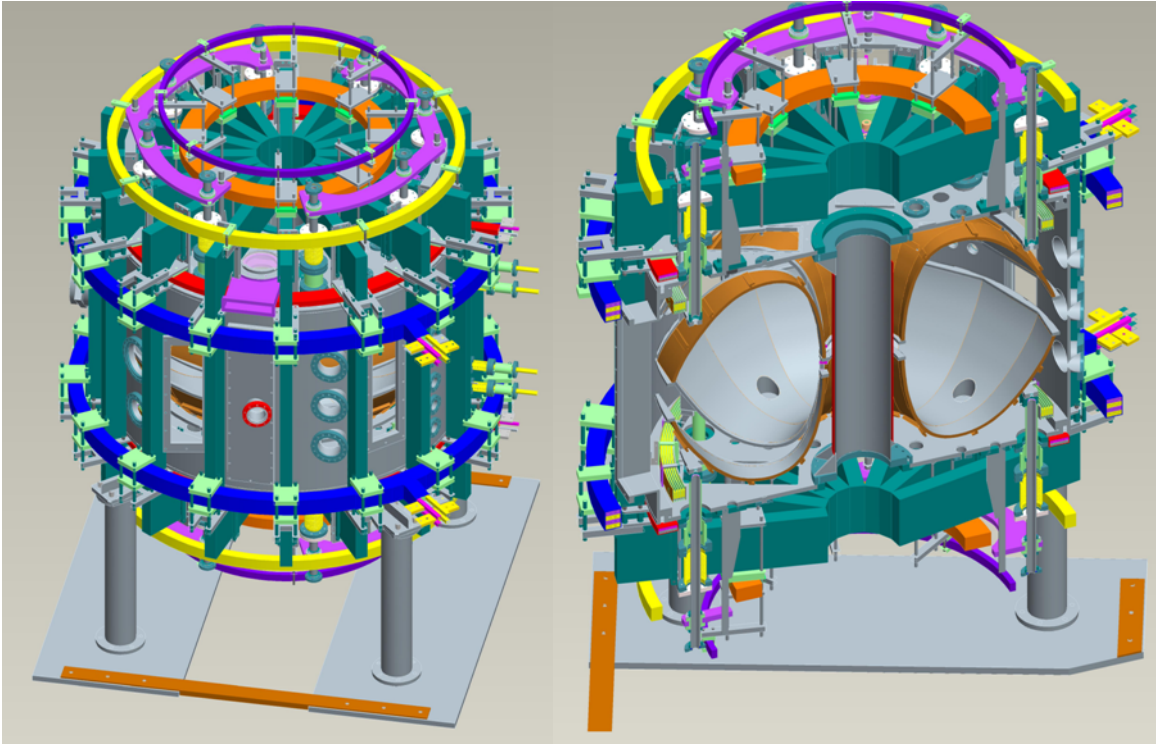


Figure 3: The Lithium Tokamak Experiment.

on the T-11M and FTU devices have studied the feasibility of using a liquid lithium limiter in tokamaks [12, 13]. Studies on NSTX using evaporative lithium deposition show increases in T_e , T_i , confinement, and MHD stability on a diverted device [14]. Many of these experiments had only a relatively small portion of the wall coated with lithium, and others were not as effective due to lithium-carbon interactions.

The Lithium Tokamak Experiment

In order to further study the low recycling regime, the Lithium Tokamak Experiment (LTX) has been constructed. Drawings of the experiment are shown in Figure 3, and machine parameters are summarized in Table 1. LTX is a spherical torus designed to nearly eliminate wall recycling. The unique feature of this device is the presence of a shell conformal to the last closed flux surface which will be coated in liquid lithium from an evaporator. The shell is made of a 3/8 inch copper layer explosively bonded to a 1/16 inch stainless steel layer, which is then plated with a layer of nickel. The shell covers approximately 90% of the plasma; two toroidal and two poloidal breaks allow plasma diagnostic views and prevent the formation of

Parameter	Value
R_0	0.40 m
a_0	0.26 m
B_T	3.4 kG
I_P	400 kA
κ	1.55
$T_{e,max}$	>300 eV
$\tau_{flattop}$	>100 ms

Table 1: LTX parameters.

large currents in the shell. The shell is resistively heated to keep the lithium in a liquid state.

Diagnostics on LTX include flux loops, Mirnov coils, a Rogowski coil, microwave interferometers, a Langmuir probe, a scanning ultraviolet spectrometer, a digital holography system, a bolometric array, Lyman- α detectors, and a Thomson scattering system. Plasmas may be fueled by a gas puffer, supersonic gas injector, or molecular cluster injector. Eventually LTX will also have a neutral beam.

The recycling rate on LTX is measured by Lyman- α detectors. These view light emitted from excited state transitions in recycled neutral atoms, such that the intensity of light is proportional to the number of neutrals present. Lyman- α detectors are used instead of Balmer- α (H_α) detectors because lithium is less reflective to light at 121.5 nm than at 656.3 nm. These measurements, along with knowledge of the particle inventory in the experiment can be used to estimate the recycling rate. For a more careful determination of this quantity, modeling using the DEGAS2 neutral particle transport code may be used.

The Thomson Scattering System on LTX

Thomson scattering is a noninvasive diagnostic technique used to measure the electron temperature and electron density of a plasma. Thomson scattering works by using the oscillating electric field of a high power laser beam to accelerate an electron, which then radiates light. The scattered light is collected by viewing optics and channeled into a spectrometer. A measurement of the Doppler broadening allows the determination of the plasma temperature, and an absolute measurement of the intensity of scattered light can be used to determine the density. The number of scattered photons N_{pe} for a given scattered wavelength λ_s is given by:

$$N_{pe} = \frac{N_i \eta T n_e r_0^2 L \Delta \Omega}{\lambda_i \delta \sqrt{\pi}} \exp\left(-\frac{(\lambda_s - \lambda_i)^2}{\lambda_i^2 \delta^2}\right) \quad (1)$$

where N_i is the number of incident photons, η is the effective detector quantum efficiency, T is the optical transmittance, n_e is the electron density, r_0 is the classical electron radius, L is the axial beam length imaged in the fiber, $\Delta \Omega$ is the solid angle collected by the fiber, λ_i is the incident wavelength, λ_s is the scattered wavelength, and $\delta = \frac{2}{c \sin \frac{\theta}{2}} \sqrt{\frac{2T_e}{m_e}}$ for scattering angle θ [15].

The Thomson scattering system on LTX [16] uses a four-stage ruby laser with energy 15 J and pulse duration 20 - 40 ns to create light at 694.3 nm. After leaving the optical table enclosure, the beam travels toward the vessel through a window angled at 7° to eliminate cavity reflections before entering an approximately 60 inch evacuated flight tube, bellows, and gate valve assembly. The beam then enters the midplane of the vessel through a gap in the shell and follows a non-radial chord across the plasma to another shell gap, where it exits the vessel through another gate valve, bellows, and flight tube assembly. A beam dump located outside the vessel vacuum absorbs the remaining light. Although not currently installed, a system of annular knife-edge baffles will be used within the flight tubes to further reduce stray light. A diagram depicting the beam path is shown in Figure 4.

The collection optics for the system are mounted on a free-standing tower assembly isolated from the vessel. A port on the top of the vessel provides a near-orthogonal view of the beam path through a BK7 window. A system of lenses images light into 16 quartz optical fibers. Each fiber carries light from one spatial channel; current measurement locations are given in Table 2. A polarized film is used to filter out stray light before it enters the viewing optics. A mounting tower allows fine adjustment of the lens and fiber positions, and allows for an overall tilt of the optics. The scattered light is brought into a grating spectrometer and then imaged onto an intensified CCD with a 512 by 512 pixel array. Notch filters may be added within the spectrometer to filter out laser light or the H_α line. A ray tracing of the collection optics is shown in Figure 5.

This system has been designed to work in an evaporative lithium environment. A stainless steel shutter protects the top viewing window from becoming coated with lithium. The shutter is attached to a rotary actuator and will only be opened for a short duration for each plasma discharge. Pneumatic gate valves at the flight tube/vessel interface operate in a similar manner. Nevertheless, should the windows become dirty, the accompanying gate valves can be closed, allowing the window to be removed and cleaned without affecting the vessel pressure.

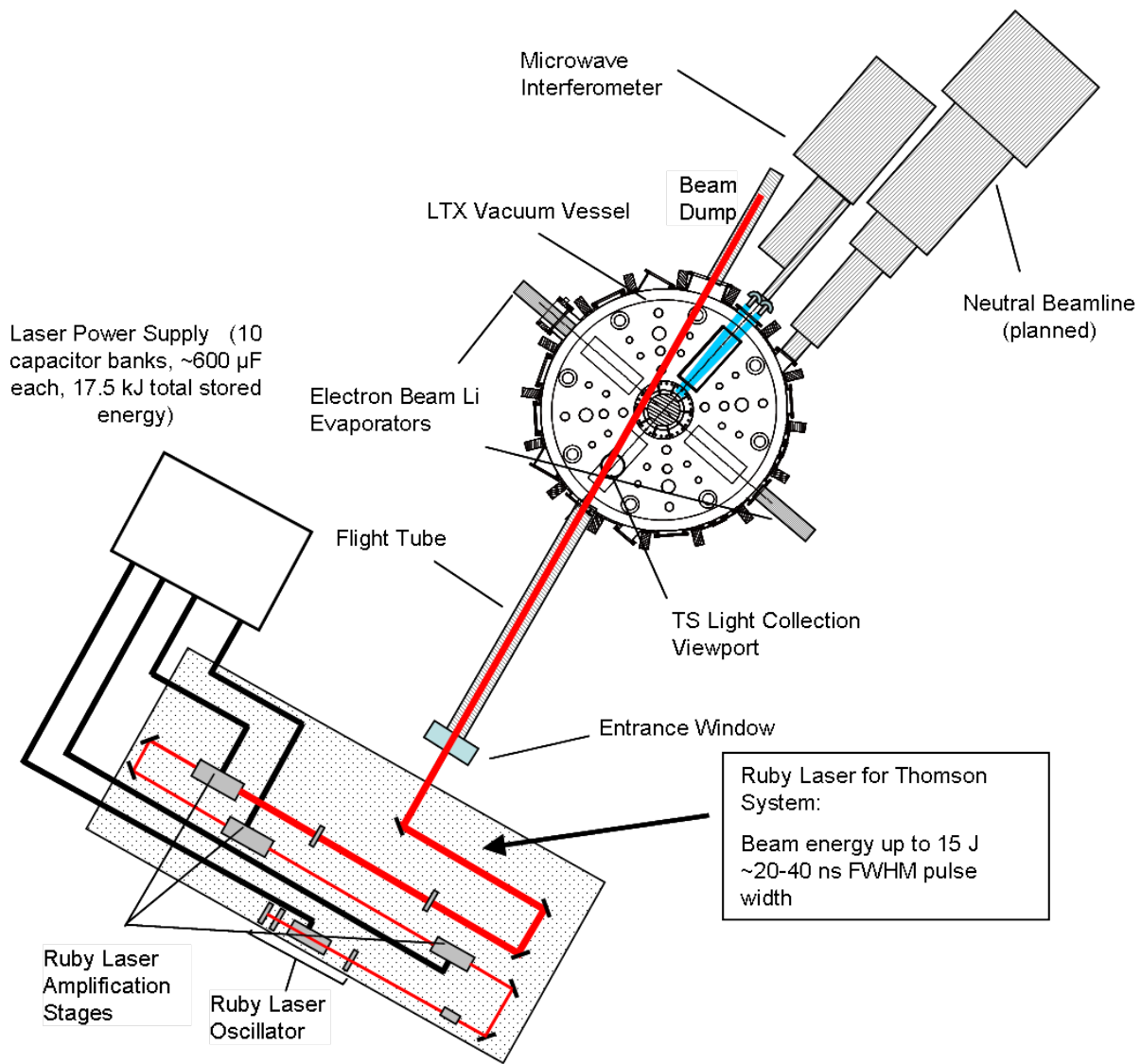


Figure 4: The Thomson scattering beam path.

Channel	R [m]	r [m]	r/a
1	0.408	0.008	0.031
2	0.418	0.018	0.069
3	0.427	0.027	0.104
4	0.449	0.049	0.188
5	0.468	0.068	0.262
6	0.488	0.088	0.338
7	0.508	0.108	0.415
8	0.529	0.129	0.496
9	0.547	0.147	0.565
10	0.567	0.167	0.642
11	0.587	0.187	0.719
12	0.608	0.208	0.800
13	0.618	0.218	0.838
14	0.628	0.228	0.877
15	0.640	0.240	0.923
16	0.650	0.250	0.962

Table 2: Thomson scattering measurement locations.

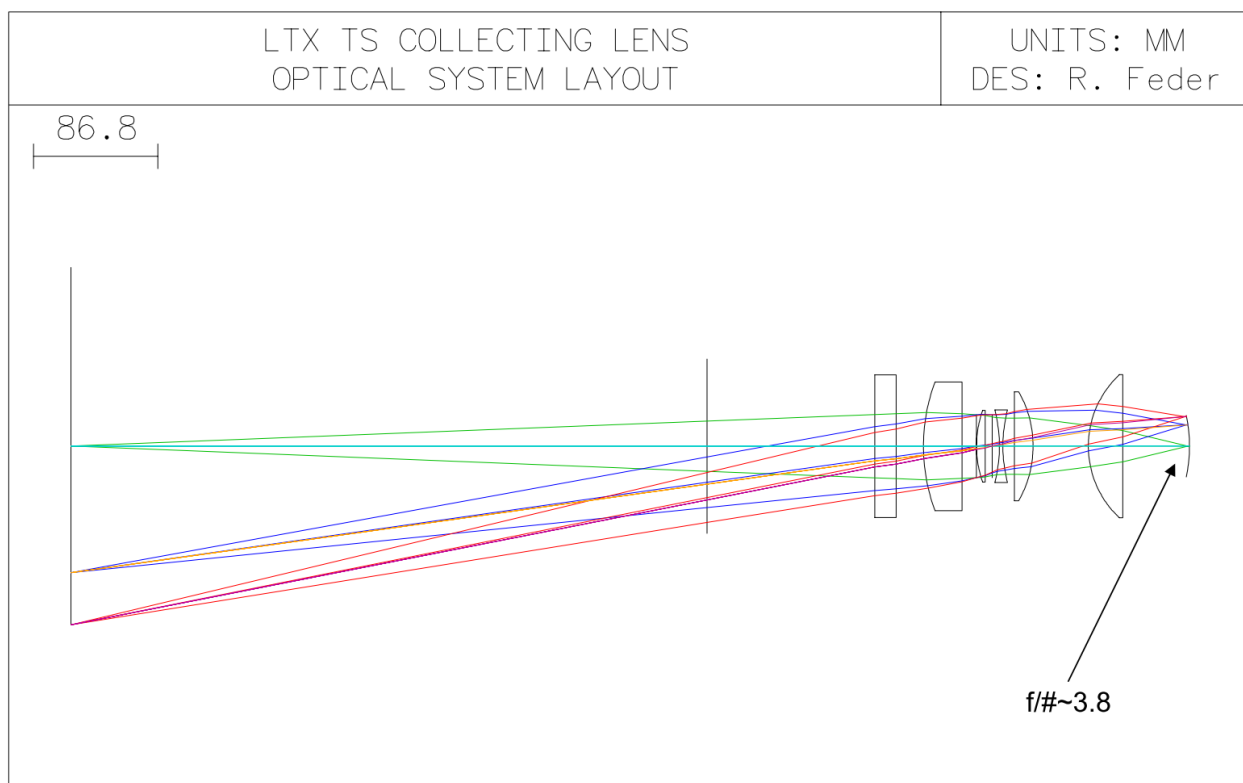


Figure 5: A ray tracing of the collection optics.

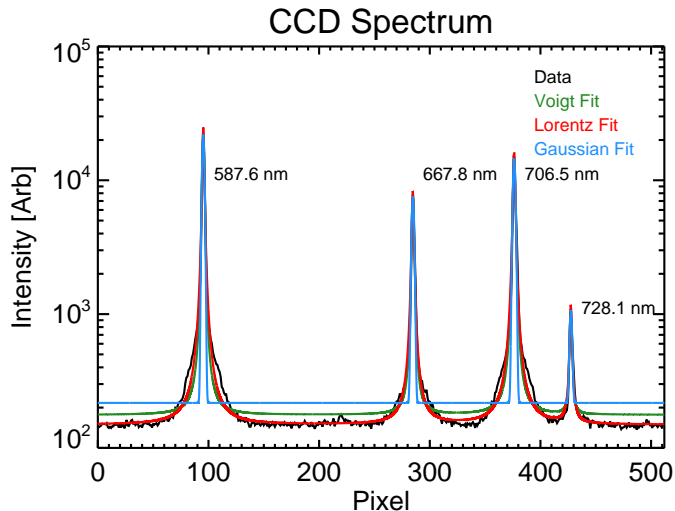


Figure 6: Helium line calibration.

Wavelength Calibration

In order to provide a one-to-one correspondence between the wavelength of incident light into the spectrometer and the CCD pixels, the system is calibrated using known emission lines from gas lamps. The N emission lines are fit to a sum of Gaussian, Lorentzian, skew-normal, or Voigt profiles¹.

The skew-normal fit, in conjunction with the H_{α} line, allows for alignment of the spectrometer. The location of the emission line is determined by fitting parameters which are matched to known emission lines from the NIST Atomic Spectra Database [18].

A rough calibration performed previously produced the following curve:

$$\lambda = \frac{1 \text{ nm}}{2.35}x + 547 \text{ nm} \quad (2)$$

where λ is the wavelength of incident light and x is the pixel number of the spectrometer. This indicates a spectral range from 547 nm to 764 nm. See Figure 6 for an example of the fit to a set of helium lines. The spectrometer has since been moved and will require another more careful calibration, along with possible tuning of the grating. Additionally, computational routines will be necessary to compensate for image curvature or other effects.

Density Calibration

In order to provide an absolute calibration of the electron density measured by the system, Raman scattering, Rayleigh scattering, or direct calibration using a known source may be used.

Raman scattering is an inelastic scattering process where photons can either gain or lose energy as they interact with molecular vibrational, rotational, and electron energy states. Scattered light is emitted in lines greater than and less than the laser wavelength, which reduces inaccuracies due to stray light. Only scattering associated with rotational state transitions is accessible to the system's spectrometer. This method of calibration works with a diatomic gas such as H_2 or N_2 , and a precision pressure gauge capable of measuring pressures at ~ 50 torr. Comparing the expected signal and the actual signal allows calibration of the efficiency of the optics.

Rayleigh scattering calibration is another option, but since the scattering occurs at the same wavelength as the laser, stray light may become a problem.

¹The Voigt profile is the convolution of the Lorentzian and Gaussian profiles of an emission line, and accounts for both the shortening of the duration of emission due to atomic collisions and the random thermal motions of the atom, respectively [17].

Completion of system, alignments, and calibrations	3 months
Data acquisition	9 months
Data analysis	9 months
Thesis writing	3 months
Total	24 months

Table 3: A highly speculative thesis timeline.

A calibrated light source such as the Labsphere URS-600 Uniform Radiance Standard may also be used to calibrate the system. This allows a more direct calibration of the system, but requires the removal of the viewing optics. This method may be used only for calibration of the spectrometer efficiency.

For plasmas expected in the experiment, the system is predicted to measure T_e with 6%-8% relative error, and n_e with 8.5%-11% relative error [16].

Goals

The Thomson scattering system on LTX is uniquely suited to measure the effects of lithium walls on plasma performance. As such, many important physics studies can be performed.

The goals of this thesis are to:

- Determine the electron temperature and its profile as a function of recycling
- Correlate the electron temperature profile peaking and the confinement
- Correlate the recycling and the edge temperature using a combination of Thomson scattering and Langmuir probe data
- Determine if the edge temperature correlates with the recycling predicted by UEDGE or other models
- Compare the response of the edge temperature and core temperature profiles in NSTX for similar recycling coefficients, if possible

In order to accomplish these goals, the construction of the Thomson scattering system must be completed. Currently, most of the hardware is in place with the exception of the final optical steering assembly and the beam dump. The system must be more carefully aligned in order to create high power beams. Absolute density and wavelength calibrations need to be performed. LTX must also begin lithium operation, which is expected within a few months.

A highly speculative timeline is given in Table 3.

References

- [1] John Wesson and D. J Campbell. *Tokamaks*. Clarendon Press, Oxford, 3rd ed edition, (2004).
- [2] M. J. Baldwin et al. *Nuclear Fusion* **42** (11), 1318–1323 (2002).
- [3] L. E. Zakharov et al. *Fusion Engineering and Design* **72** (1-3), 149–168 November (2004).
- [4] D. K. Mansfield et al. *Physics of Plasmas* **2** (11), 4252–4256 November (1995).
- [5] D. K. Mansfield et al. *Physics of Plasmas* **3** (5), 1892–1897 May (1996).
- [6] G. L. Jackson et al. *Journal of Nuclear Materials* **241-243**, 655–659 February (1997).
- [7] R. Kaita et al. *Fusion Engineering and Design* **61-62**, 217–222 November (2002).
- [8] R. Majeski et al. *Journal of Nuclear Materials* **313-316**, 625–629 March (2003).

- [9] R. Majeski et al. *Fusion Engineering and Design* **72** (1-3), 121–132 November (2004).
- [10] R. Majeski et al. *Nuclear Fusion* **45** (6), 519–523 (2005).
- [11] R. Majeski et al. *Physical Review Letters* **97** (7), 075002–4 (2006).
- [12] S. V. Mirnov et al. *Plasma Physics and Controlled Fusion* **48** (6), 821–837 (2006).
- [13] M. L. Apicella et al. *Journal of Nuclear Materials* **363-365**, 1346–1351 June (2007).
- [14] H. W. Kugel et al. *Physics of Plasmas* **15** (5), 056118–13 May (2008).
- [15] N. Bretz et al. *Applied Optics* **17** (2), 192–202 (1978).
- [16] T. Strickler et al. *Rev. Sci. Instrum.* **79**, 10E738–5 October (2008).
- [17] Eugene Hecht. *Optics*. Addison-Wesley, Reading, Mass, 4th edition, (2002).
- [18] http://physics.nist.gov/PhysRefData/ASD/lines_form.html.